Surface & Coatings Technology 253 (2014) 139–147

Contents lists available at ScienceDirect

Surface & Coatings Technology

journal homepage: www.elsevier.com/locate/surfcoat

Interfacial fracture mechanism associated with mixed oxides growth in thermal barrier coating system

Rong Xu, Xue Ling Fan, Wei Xu Zhang, T.J. Wang *

State Key Laboratory for Strength and Vibration of Mechanical Structures, Department of Engineering Mechanics, School of Aerospace Engineering, Xi'an Jiaotong University, Xi'an 710049, China

ARTICLE INFO

Article history:
Received 17 October 2013
Accepted in revised form 14 May 2014
Available online 27 May 2014

Keywords:
Delamination
Thermal barrier coating
TBCs
Finite element method

ABSTRACT

The interfacial failure mechanism of the thermal barrier coating system (TBCs) was numerically investigated by considering the role of mixed oxides (MO), which was induced by the discontinuous α-Al_2O_3 at the interface between top and bond coatings. It is shown that MO has a significant effect on the interface integrity. High growth rate of MO will induce the initiation and propagation of interface cracks and eventually results in the debonding of ceramic coating. The high coverage ratio of MO at the interface will accelerate the propagation of an interface crack. Therefore, suppressing the formation of MO can effectively improve the durability and performance of TBCs. The results obtained herein can well explain some previous observations in the thermal shock experiments of TBCs and could offer the potential for improving the durability of TBCs.

1. Introduction

The increased thermal efficiency of advanced gas turbine is always associated with the dramatic increase of the turbine entry temperature. This high inlet temperature may induce the premature failure of turbine components, especially the turbine blades. Thus, an excellent thermal protection system for turbine blades is of the essence. The thermal barrier coating system (TBCs), commonly consisting of an yttria partially stabilized zirconia ZrO_2–8%Y_2O_3 ceramic top coat (TC) and a metallic bond coat (BC) deposited onto a superalloy substrate, is widely used as a thermal insulation system to protect gas turbine blades from oxidation, corrosion, etc. [1,2].

There are many damage mechanisms for materials and structures [3–6]. Spallation of TC caused by interface debonding is one of the major failure mechanisms in TBCs [7–11]. Experimental and numerical results show that a thermally grown oxide (TGO) layer forming at the interface of BC and TC during high temperature operation plays an important role in the failure of TBCs [12–15]. During the service, the thickness of TGO increases with the thermal exposure time, which has a strong influence on the stress distribution within TC, TGO, BC and their interface [16–18].

Various constituents of TGO have been observed recently [14,19] including α-Al_2O_3, Cr_2O_3, NiO, and (Ni, Co) (Cr, Al)$_2O_4$ (spinels), which have different effects on the failure mechanisms of TBCs. With the uniform and dense microstructure and low growth rate, α-Al_2O_3 formed at the TC/BC interface is desirable for the durability of TBCs [20] since it contributes to the protection for BC from further oxidation. Moreover, the low growth rate of α-Al_2O_3 has less potential to induce high growth stress in TBCs. Usually, Cr_2O_3, NiO and (Ni, Co)(Cr, Al)$_2O_4$ (spinels) are referred as mixed oxides (MO) [21–24]. The MO has a deteriorating effect on the protection of BC and the integrity of the interface [19,25], which is related to the undesirable microstructure and material property of MO. For example, the growth rate of NiO in the air at 1100 °C is three times higher than that of α-Al_2O_3 [26]. Clearly, the high growth rate of NiO may easily result in a high level stress in TBCs. Spinels, usually stoichiometrically expressed as (Ni, Co)(Cr, Al)$_2O_4$, are porous and brittle and also have a high growth rate, which are greatly harmful to the integrity of the TC/BC interface [20]. In addition, MO exhibits a worse adhesion to the ceramic coating. Therefore, MO is regarded as the most undesirable oxides at the TC/BC interface.

More recently, investigations focus on the effects of MO. Chen *et al.* [27] observed that when exposed in a low-pressure oxygen environment the formation of MO can be partially or fully suppressed, which is useful to increase the durability of TBCs. To investigate how MO affects the durability of TBCs, Li *et al.* [23] prepared a series of TBCs specimens deposited under different conditions, and they confirmed the deteriorative effect of MO on TBCs durability. Also, they revealed the qualitative relationship between the surface coverage ratio of MO and the lifetime of TBCs.

It is shown in the previous thermal shock experiments that there is a relationship between the lifetime of TBCs and the contents of MO at the TC/TGO interface [18,22,23]. However, it is still unclear how the MO growth affects the stress distribution and damage evolution at the TC/TGO interface, and then results in the eventual interfacial delamination. The objective of this work is to numerically investigate the effect of MO growth on the interfacial fracture mechanisms of TBCs such as the stress distribution, crack initiation and propagation. It is important for the engineers to predict the stress distribution and damage evolution in TBC, which is usually unavailable in real TBC thermal experiments.

* Corresponding author.
E-mail address: wangtj@mail.xjtu.edu.cn (T.J. Wang).

http://dx.doi.org/10.1016/j.surfcoat.2014.05.026
0257-8972/

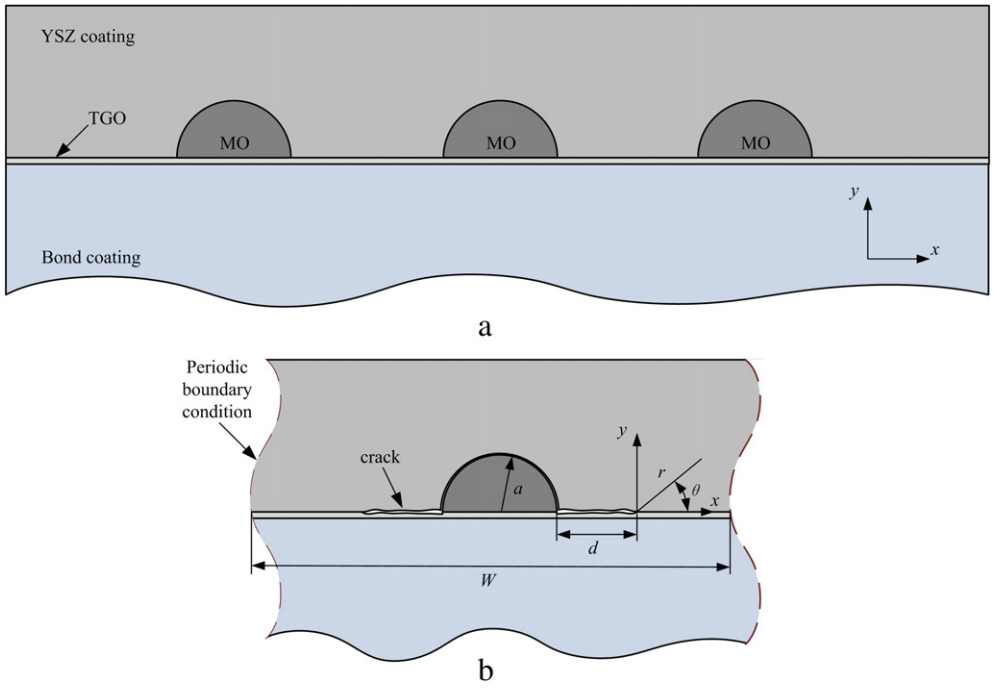

Fig. 1. (a) The TBCs model with MO at the TC/TGO interface. (b) Simplified cell model with local coordinates of an interface crack.

In Section 2, the problem is formulated, in which the physical model, the material models and fracture criterion are presented. In Section 3, the numerical procedures are presented. In Section 4, the effects of surface coverage ratio and growth rate of MO on the interfacial failure mechanism of TBCs are presented and discussed in detail. The concluding remarks are presented in Section 5.

2. Formulation of the problem

A typical TBCs consists of four layers: TC, TGO, bond coat (BC), and superalloy substrate. So, two-dimensional plane strain model is adopted to investigate the interface fracture behavior of TBCs, as shown in Fig. 1(a). The TC consists of yttria partially stabilized zirconia ZrO_2–8%Y_2O_3 and the BC on the Ni-based superalloy substrate consists of MCrAlY. The thicknesses of the substrate, BC and TC are 30 mm, 0.1 mm, and 0.5 mm, respectively, for ZrO_2–8%Y_2O_3 TBCs. To analyze the effect of MO on the interfacial fracture of TBCs, TGO is decomposed into two components, i.e. α-Al_2O_3 and MO (Cr_2O_3, NiO, and spinel). The α-Al_2O_3 regarded as a flat layer between TC and BC is the dominant component of TGO.[¶] The MO, an isolated and semi-circle domain, locates at the TC/TGO interface and penetrates into the TC. Unless otherwise stated, the initial thickness of TGO is 2 μm and the ratio of initial MO radius to TC thickness (a/h_{TC}) is 0.4.

As discussed earlier, the coverage ratio of MO at the TC/TGO interface is a key parameter and should be considered, which is defined as,

$$\kappa = \frac{2a}{W} \tag{1}$$

The debonding ratio of the interface is defined as

$$\eta = \frac{2(a+d)}{W} \tag{2}$$

where a is the radius of MO, W is the width of the cell and d is the length of the interface crack.

[¶] In what follows, the TGO is particularly referred to the dominant component α-Al_2O_3.

2.1. The material models

In multiple-layer TBCs model, it is assumed that each layer is homogeneous, isotropic, elastic and viscous materials. The thermo-elastic properties of the each layer are presented in Table 1 [28–31]. Note that all these layers obey Norton power-law of creep, i.e. $\dot{\varepsilon}_{cr} = B\sigma^n$ where $\dot{\varepsilon}_{cr}$ is the strain rate (s^{-1}) and σ is the stress (MPa). The material constants B and n are temperature independent as listed in Table 1.

The TGO and MO growth behaviors at the holding time of high temperature (1200 °C) are simulated and regarded as the crucial factors to the interface failure of TBCs. The oxide growth is presented by a user subroutine *UEXPAN* in ABAQUS code [32], imposing a growth strain that contains two parts: ε_t and ε_g. For TGO, ε_t is normal to the TGO/BC interface and ε_g is parallel to the interface [12]. The growth strain is assumed to vary within the experimentally determined range of $10^{-4} < \varepsilon_g < 5 \times 10^{-3}$, and the thickening strain is usually considered as one-tenth of the growth strain [12,33]. Herein, ε_g is treated as a constant value of $\varepsilon_g = 2.4 \times 10^{-3}$. For MO growth, a homogeneous growth rate ε_u is assumed, i.e. growth strain ε_g and thickening strain ε_t are equal to ε_u. To investigate the effect of MO growth on the interface failure of TBCs, ε_u is treated as a variable with the initial value of ten times of ε_g and then is set to twenty times and thirty times of ε_g [26], respectively.

It should be noted that the growth rate of TGO is much smaller than that of MO [26], and it seems that the thickening of the TGO layer may not induce a considerable increase of stress at the interface. While MO growth results in a huge normal stress, which plays an important role in the interfacial delamination of TBCs. Therefore, MO growth is regarded as essential to the interfacial delamination. Certainly, the rough TGO layer would induce totally different results, which will be discussed in the future work.

2.2. Interface fracture criterion

Due to the complexity of stress distribution on the interfaces of TC/TGO and TC/MO caused by MO growth, finite element calculations are performed by using the commercial ABAQUS code, in which a stress-based criterion is employed. The criterion says that interfacial

Table 1
The thermal–elastic properties of TBCs components.

Component	Young's modulus, E (GPa)	Poisson ratio, ν	Thermal expansion coefficient (CTE), α ($10^{-6}K^{-1}$)	$B(s^{-1}MPa^{-n})$	n
TC	50	0.1	9–11	$1.8e^{-9}$	1
MO	100	0.3	5–8	$5e^{-9}$	1
TGO(α-Al_2O_3)	350	0.3	6–9	$7.3e^{-9}$	1
BC	200	0.3	12–17	$2.15e^{-8}$	2.45
SUB	210	0.3	12–15	$2.25e^{-9}$	3

debonding initiates as the parameter f at a characteristic distance ahead of the crack tip equals to one [36,37].

The parameter f is defined as [32]

$$f=\sqrt{\left(\frac{\hat{\sigma}_n}{\sigma^f}\right)^2+\left(\frac{\tau_1}{\tau_1^f}\right)^2+\left(\frac{\tau_2}{\tau_2^f}\right)^2},\hat{\sigma}_n=\max(\sigma_n,0) \tag{3}$$

where σ_n is the normal component of local stress across the interface at the specified distance, τ_1 and τ_2 are the shear stress components, and σ^f, τ_1^f and τ_2^f are the normal and shear failure stresses, respectively.

In the case of two-dimensional analysis, the second component of the shear stress τ_2 equals zero. Therefore, for the present two-dimensional problem, the critical stress criterion can be simplified as

$$f=\sqrt{\left(\frac{\hat{\sigma}_n}{\sigma^f}\right)^2+\left(\frac{\tau_1}{\tau_1^f}\right)^2},\hat{\sigma}_n=\max(\sigma_n,0) \tag{4}$$

3. Numerical calculations

Considering the periodicity of multilayer TBCs, a unit cell model shown in Fig. 1(b) is constructed to investigate the initiation and propagation of an interface crack around the MO. For the numerical calculations, nodes are allocated in pair at the left and right boundaries of the unit cell model with periodic boundary conditions [10,34] applied to keep the opposite edges deform parallel in a tangential sense.

Also, the local coordinates of the interface crack are shown in Fig. 1(b). The crack flank displacements (δ_1, δ_2) and stress fields (σ_{12}, σ_{22}) with a distant r ahead of the interface crack tip can be written as [35],

$$\delta 2+i\delta 1=\frac{8}{(1+2i\varepsilon)\cosh(\pi\varepsilon)}\frac{K}{E^*}\left(\frac{r}{2\pi}\right)^{1/2}r^{i\varepsilon} \tag{5}$$

$$\sigma_{22}+i\sigma_{12}=K(2\pi r)^{-1/2}r^{i\varepsilon} \tag{6}$$

where $1/E^*=\frac{1}{2}\left(1/\overline{E1}+1/\overline{E2}\right)$, $i=\sqrt{-1}$, and $r^{i\varepsilon}=\cos(\varepsilon\ln r)+i\sin(\varepsilon\ln r)$ with $\varepsilon=\frac{1}{2\pi}\ln\frac{1-\beta}{1+\beta}$ representing the singularity of the crack tip field. K is the complex stress intensity factor (SIF) and can be obtained through the J-integral around crack tip by using finite element method (FEM). According to the crack stress field and the fracture criterion, one can analyze the initiation and propagation of the interface crack.

The propagation of a pre-existent crack at the TC/TGO interface can be simulated by using the "Debond" tool in ABAQUS/Standard code [32], as shown in Fig. 2, in which the separation of adjacent surfaces can be predicted. The stress at a constant distance ahead of the crack tip is considered as a pertinent value in the criterion, which can be optimized to neglect the effects of crack tip singularity (1 to 3 elements) [38], as shown in Fig. 2. Indeed, to verify the reliability of numerical solutions for the problem studied herein, the convergence of mesh configuration and characteristic distance has been checked before the normal computations.

The previous investigations [39,40] have shown that the MO/TC interface has a weak strength while the TC/TGO interface has a strong one. So, we can choose the critical normal stress for the interfaces of TC/MO and TC/TGO being 20 MPa and 200 MPa, respectively [8,17,39].

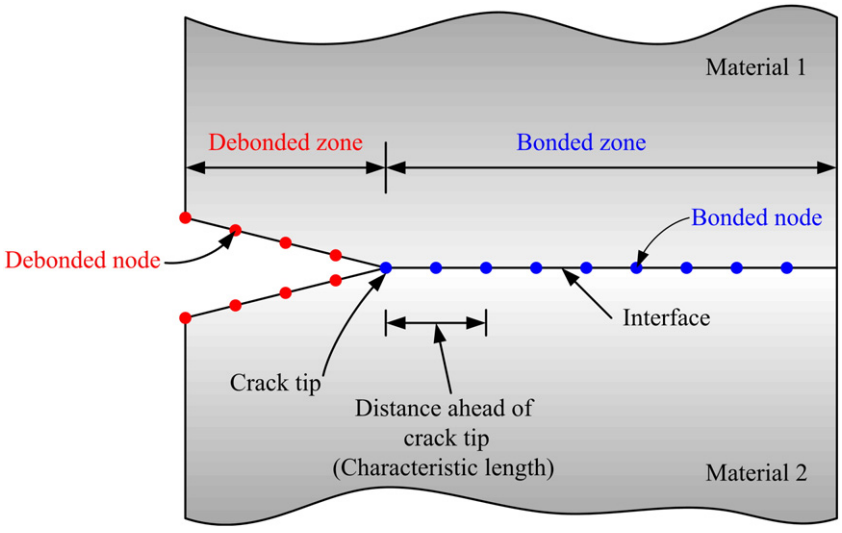

Fig. 2. Schematic illustration of"debond"technique adopted to simulate interface crack propagation.

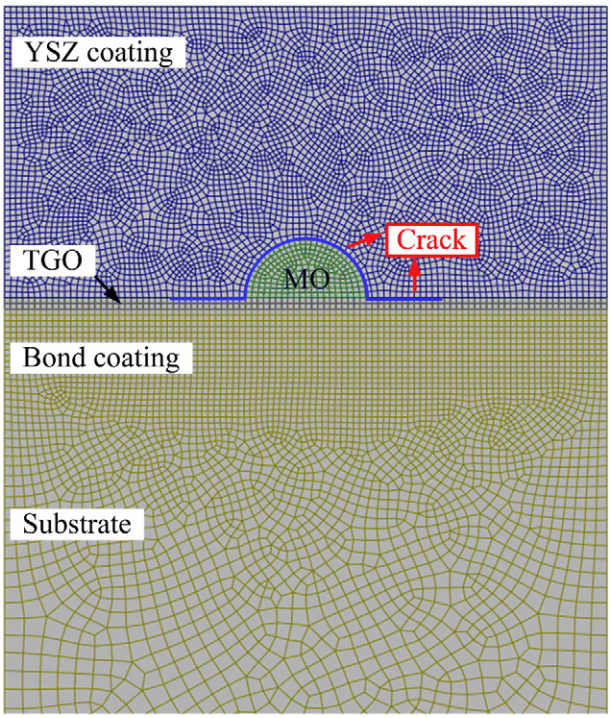

Fig. 3. Finite element model of TBCs with a typical mesh along the predetermined crack path.

On the other hand, it is observed that the normal stress σ_{22} perpendicular to the interface can be used to accurately predict the propagation of the interface crack and eventually the coating debonding [30,40]. Therefore, we assume that the shear stress almost has no effect on the interface fracture, which may slightly overestimate the lifetime of TBCs. Non-uniform meshes are adopted in the finite element calculations, as shown in Fig. 3. The four-node bilinear plane strain quadrilateral reduced integration elements are selected for all the layers. To ensure the calculation accuracy, very fine meshes along the pre-determined interface crack path are used.

It is well known that the ceramic coating surface in TBCs is directly exposed to the hot gas in the turbine, so there is a gradient distribution of temperature in the thickness direction of TBCs. Herein, we consider a homogeneous distribution of temperature to simplify analysis. This simplification appears to slightly overestimate the effect of MO growth on the interfacial delamination. The total thermal loading time is T and the thermal loading history consists of three stages, as shown in Fig. 4. Firstly, the model is imposed to ambient temperature gradient from 20 to 1200 °C in $T_h = 100$ s. In this stage, the thermal stress induced by the CTE mismatch of layers dominates the stress distribution. Then, to simulate the working environment of the blades in a gas turbine

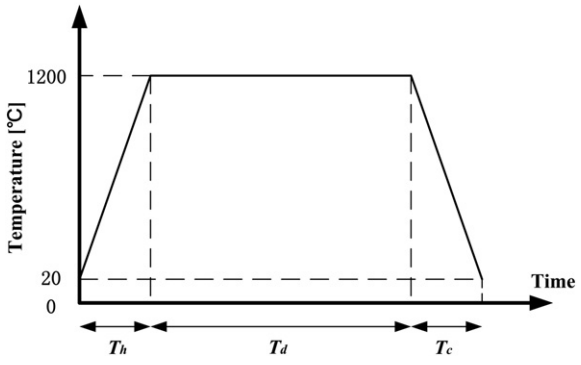

Fig. 4. The thermal loading condition used in FEM simulation.

the ambient temperature is maintained at 1200 °C for a sufficient long dwell-time $T_d = 8000$ s. During the dwell-time T_d, the TGO and MO grow, respectively. Finally, the model is imposed to a decreasing ambient temperature from 1200 to 20 °C. This cool stage is regarded as the contrary counterpart of the heating stage. The cooling time T_c is equal to the heating time T_h.

4. Results and discussions

4.1. Interface failure associated with MO growth

The initiation and propagation of interfacial delamination consist of three stages, as shown in Fig.5. At first, the weak interface of MO/TC debonds as the heating process continues, which is induced by the mismatch stress of different components especially that of MO and TC [28,29]. As might be intuitively expected, the expansion of MO with low CTE and TC with high CTE can induce considerable tensile and shear stresses around MO, and then the weak interface of MO/TC could be delaminated. It should be noted that the debonded MO/TC interface makes a great contribution to the eventual spallation failure of TBCs. This is because the debonding could result in an analogous buckling behavior during the subsequent heating process [41]. Also, the analogous buckling could induce a compressive zone in TC and a tensile zone across the interface, as shown in Fig.5 step A, in which the normalized loading time t/T is about 0.0144. Therefore, a pre-tensile stress exists at the crack tip of TC/TGO interface before MO growth,[§] which is undoubtedly detrimental to the interface property. This observation is consistent with the results of He *et al.* [41–43]. Secondly, TBCs is imposed to a constant temperature about 1200 °C during the dwell period, where MO and TGO are oxidated simultaneously. In this stage, the thickening of the TGO layer has a negligible influence on the normal stress distribution at the interface. The fast growth of MO perpendicular to the circumference results in the increase of tensile stress at the TGO/TC interface and then plays a major role in the subsequent interfacial delamination. In detail, the normal stress σ_{22} in the tensile zone (the crack tip of TGO/TC interface) increases continuously with enlarging of MO until it reaches the critical strength, as shown in Fig.5 step B, in which the normalized loading time t/T is about 0.3228. Meanwhile, MO growth will induce a compressive zone in the YSZ coating above the protruding MO and the magnitude of this compressive is determined by the growth rate of MO, as shown in the stress distribution of Fig.5 step B. Interestingly, these tensile and compressive zones have been predicted by the experiment of Li et al. [23]. They stated that there is a compressive force acting on the YSZ coating by the local protruding MO at the YSZ/bond coat interface and the higher the growth rate the higher the compressive force, which is in agreement with the present numerical results. Sequentially, the interfacial delamination initiates and extends with the growth of MO once σ_{22} ahead of the interface crack tip reaches the critical strength, as shown in Fig.5 step C, in which the normalized loading time t/T is about 0.7480. Obviously, in the last two stages, a compressive state appeared in MO and TC deforms like a film being jacked up by an inclusion from the substrate. Therefore, this work would be an important consideration in the practice applications where the interfacial failure emerges in the film/substrate system caused by an inclusion at the interface. Interestingly, this simulation can be demonstrated by the experimental results of Ali et al. [21,44]. In their experiments about the degradation of TBCs due to thermal cycling up to 1150 °C, crack initiated and propagated in the MO near the YSZ coating and mixed oxide increased its thickness until the spallation of the YSZ top coating. The crack propagation path shown in their scanning electron micrographs fits well with the present numerical predictions shown in Fig.5. Moreover, we can obtain the stress distribution before and during the spallation of the YSZ top coating, as shown in Fig.5.

[§] MO growth is considered during the process of heating dwell. So in this stage MO growth plays an ignorable role in debonding.

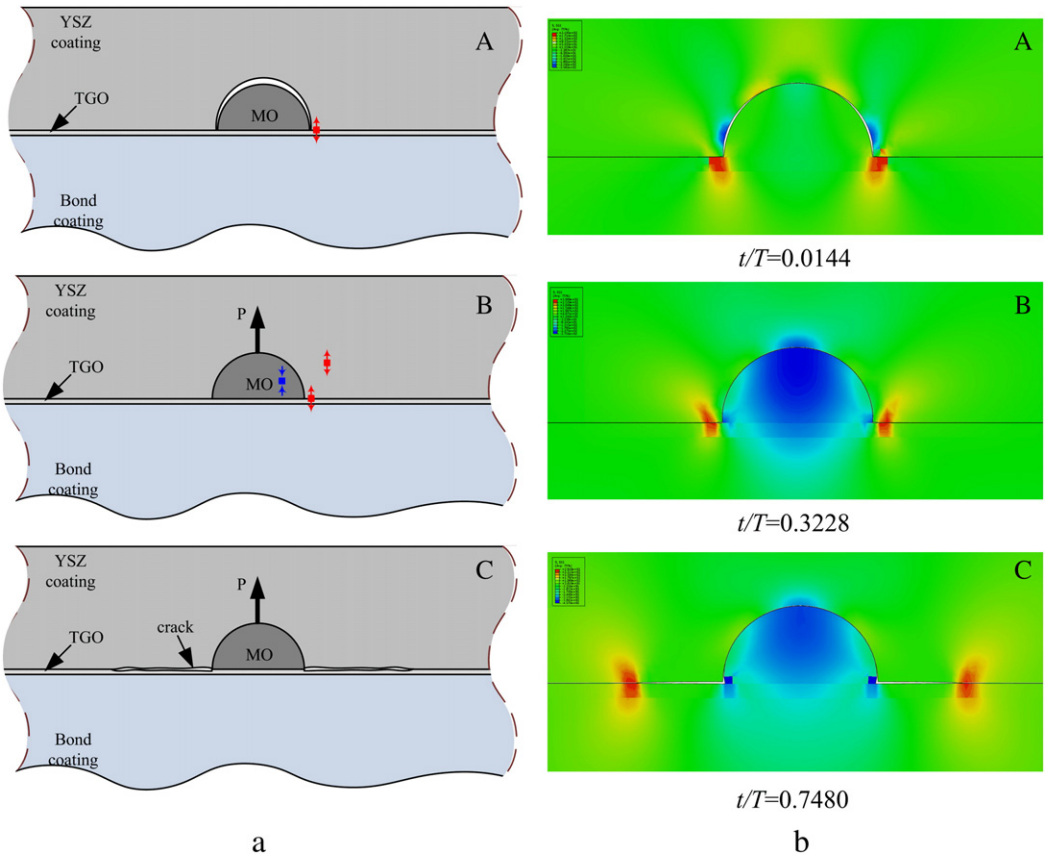

Fig. 5. The interface failure behavior associated with the MO growth: (a) schematic of the growth of the MO and the interfacial delamination; (b) the normal stress distribution around the MO. In the first stage, the thermal expansion dominates the interface failure. The low CTE of MO and a high CTE of TC induce a tensile force at the MO/TC interface and subsequent debonding(stage A). In the second stage, the MO growth plays a great role in the interface failure. The growth of MO jacks the TC up and induces the tension stress at the TGO/TC interface (stage B). Then, interfacial delamination appears if the tension stress exceeds the interfacial strength (stage C).

This stress distribution can act as mechanical description and explanation for the failure of TBCs in the experimental results of Ali et al. [21,44] and provide a better understanding of the failure mechanism caused by MO growth.

Spallation of the ceramic coating caused by the convergence of the interface crack in services is a significant factor that limits the application and improvement of TBCs. Fig. 6 schematically shows the coalescence of interface cracks emanating from the tip of neighboring MO and the corresponding normal stress distributions. Also, Fig. 6 shows the whole failure process of TBCs including interface crack initiation, propagation and coalescence, and final spalling of ceramic coating.

To obtain a quantitative understanding of the effect of MO growth on the interfacial delamination, we show the variation of interface crack length as a function of the normalized time in Fig. 7 for different MO growth rates. Fig. 7 shows that the interface crack propagates more dramatically for high growth rate of MO, which indicates that the interfacial delamination is promoted by the high growth rate of MO. It is generally accepted that MO (Cr_2O_3, spinel ($(Ni, Co)(Cr, Al)_2O_4$)) has high growth rate and it would be accelerated if large ingredient of NiO is contained within MO, leading to an extremely high growth rate [23,26]. In contrast, a dense TGO mainly consisting of α-Al_2O_3 has a much lower growth rate, which is even lower than the lowest growth rate presented in Fig. 7. Thus it is obvious that the growth of MO is detrimental to the interface integrity, and higher growth rate of MO will deteriorate the interface integrity more seriously. Conceivably, this result can be verified by the experiments of Ali et al. [21], in which the substantial increase in the oxidation rate easily led to the formation of cracks and induced the spallation of the TBCs. This result has also been demonstrated by experiments [23,27]. Our result also implies that if the component of TGO is only α-Al_2O_3, the potential of interface delamination is very low even though the geometry imperfections of the interface appeared. Therefore, improvement of the deposition technique and pre-treatment process to form a uniform continuous α-Al_2O_3 at the TC/BC interface is strongly recommended for improving the durability of TBCs.

4.2. Effect of the surface coverage ratio of MO

It is of interest to note that a marked rise in the slope of some curves in Fig. 7 appears as the length of the interface crack reaches a critical value. It indicates that the propagation velocity of delamination increases dramatically once a sufficient length of crack is reached. This accelerating behavior generally occurs in the case of TBC with a small MO space (e.g. $W/h_{TC} = 1$). It implies the effect of MO space on the interfacial delamination of TBCs, which corresponds to the various coverage ratios of MO. It is clear from Fig. 7 that interfacial delamination initiates in the region of normalized loading time between 0.2 and 0.3 for larger space of MO (e.g. $W/h_{TC} = 4$ and 2, which corresponds to a relatively few MO at the interface). However, the interface crack occurs earlier for the relatively small value of MO space (e.g. $W/h_{TC} = 1$). As shown in Fig. 7(c), the TGO/TC interface begins to delaminate at certain normalized loading time. Therefore, it is concluded that interfacial failure emerges earlier for the TBCs with a larger MO space at the interface.

As mentioned above, MO space has a strong influence on the interfacial delamination of TBCs, especially on the coalescence of interface cracks. To explore the effects of MO space on the interfacial delamination, the interface crack length is plotted as a function of the normalized time for different MO space, as shown in Fig. 8. It is seen that a smaller MO space (e.g. $W/h_{TC} = 1$, 1.2 and 1.5) accelerates the propagation of interface cracks. Furthermore, for different MO space the interfacial

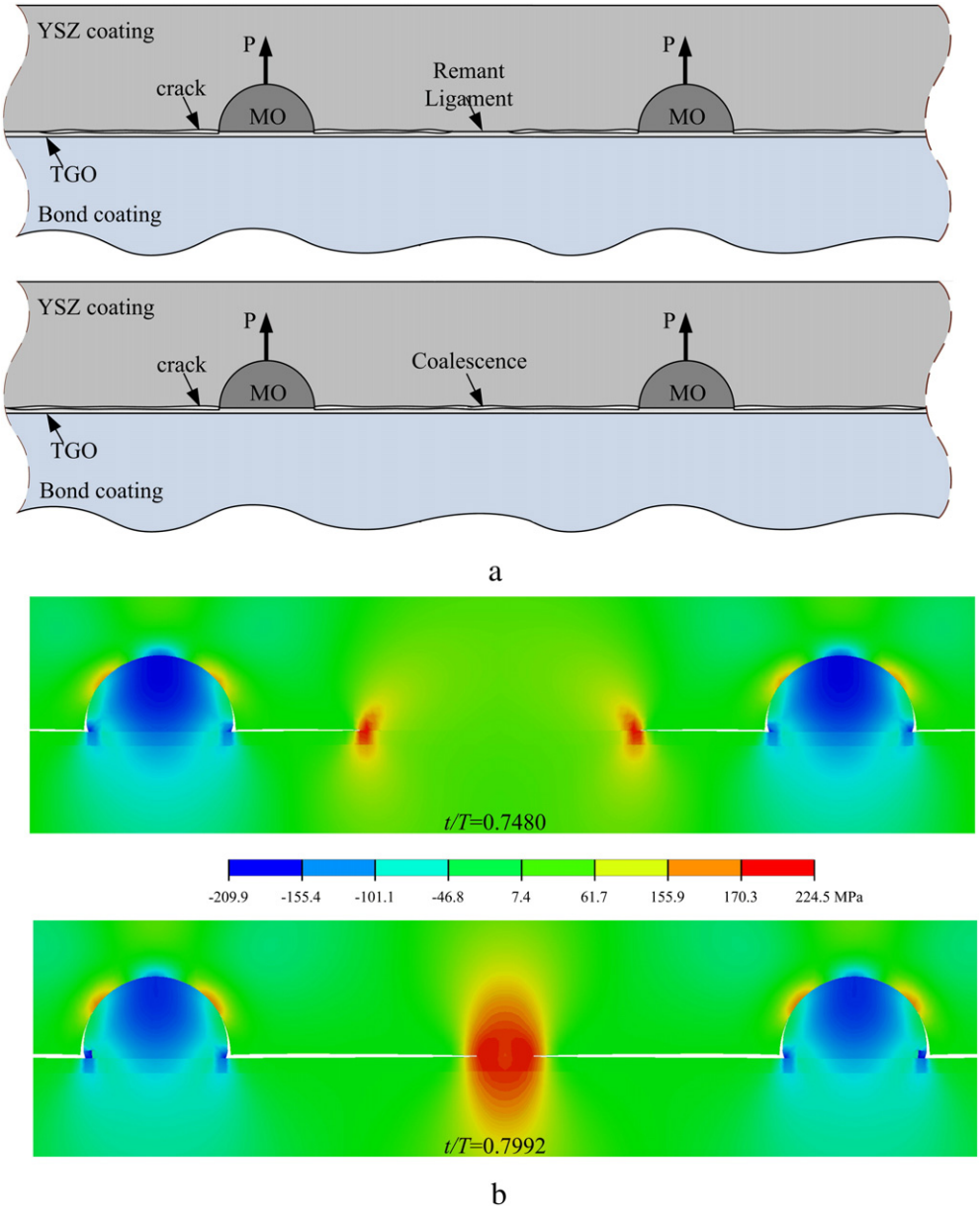

Fig. 6. The coalescence of interface cracks emanating from the tip of neighboring MO. (a) Schematic of the coalescence of interface cracks; (b) the normal stress distribution during coalescence.

delamination accelerates sharply at obviously different normalized loading time. For the smallest MO space (e.g. $W/h_{TC} = 1$), the interface crack increases dramatically at the normalized loading time 0.293. Subsequently, the interface crack propagates at a high velocity until the neighboring cracks coalesce and then the spalling of TC occurs. The final spalling state corresponds to the last numerical data points on the curves in Fig. 8. Herein, earlier accelerated propagation and then high propagating velocity of the interfacial delamination imply that small distance of neighboring MO may result in a premature interface failure of TBCs. However, in the case of relatively large MO space, the propagation of the interface crack appears to be postponed (e.g. $W/h_{TC} = 1.5$ and 2) and even be suppressed (e.g. $W/h_{TC} = 3$, 4 and 6) for a given normalized loading time. It indicates that the TBCs with a large MO space have a high tolerance to the interfacial delamination. Therefore, the present numerical results can well explain the previous experimental observations that the lifetime of TBCs decreases dramatically for a large ratio of MO [18,21,23].

Furthermore, Fig. 8 suggests that there exists an asymptotic curve of crack length for large MO space (e.g. $W/h_{TC} = 3$, 4 and 6), which indicates that the difference between the evolution of interface crack length can be neglected for the TBCs with sufficiently large MO space under certain load condition. On the other hand, there may be a critical value of MO space, below which the propagation of the interface crack will be accelerated. As pointed out earlier, the propagation of the interface crack will be accelerated once the crack length reaches about 0.2 mm for the smallest MO space (e.g. $W/h_{TC} = 1$) studied herein. In comparison, for relatively larger MO space (e.g. $W/h_{TC} = 2$), the interface crack propagates steadily until it extends to 1.6 mm. This interestingly implies that the critical MO space may be determined by the current length of the interface crack.

To clarify the effect of the current length of the interface crack on the critical MO space, we plot the normalized failure time as a function of the normalized distance of MO for different non-dimensional current crack lengths, as shown in Fig. 9. As expected, there is a stable value of spalling time, as shown in Fig. 9, for sufficiently large MO space, e.g. $W/h_{TC} = 3$ to 6. This stable behavior indicates that if MO space reaches a critical value, approximately two times of the film thickness, i.e. $W/h_{TC} \geq 2$ for the smallest interfacial delamination ($\bar{d} = 0.04$)

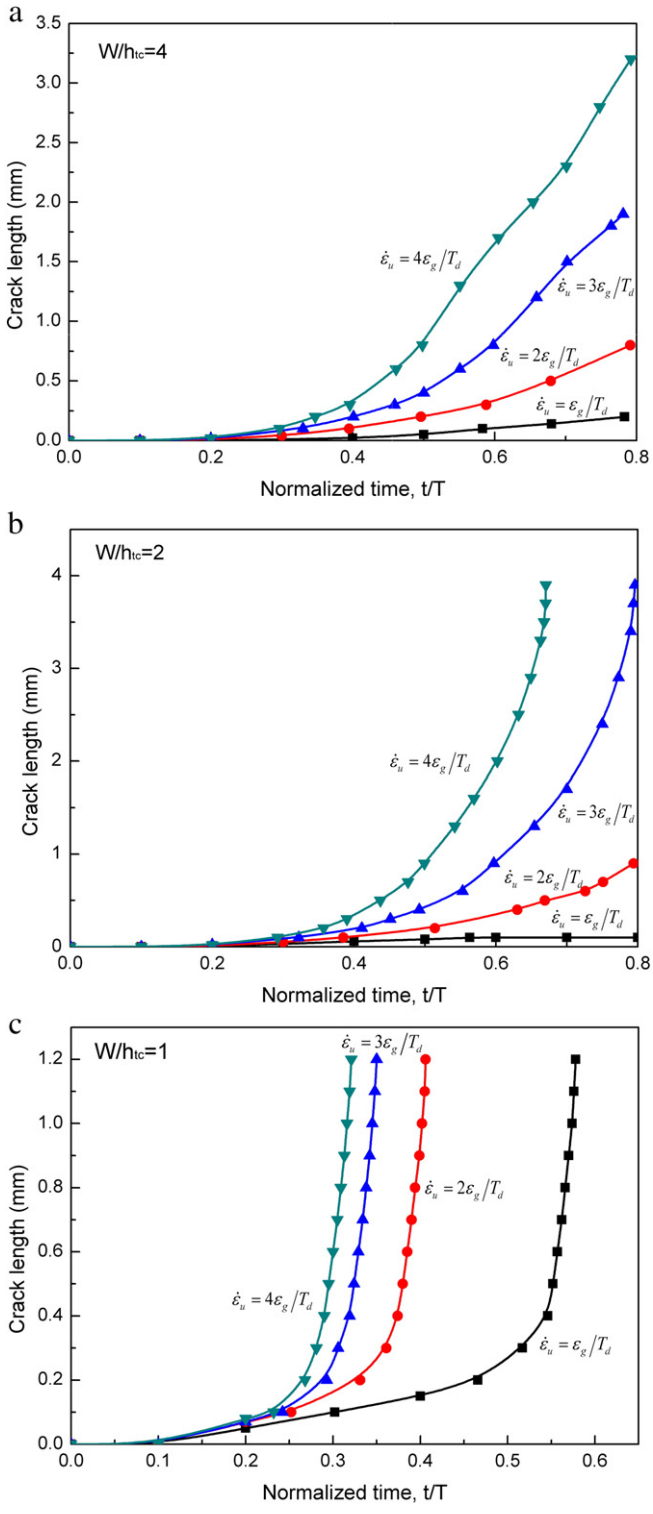

Fig. 7. The interface crack length as a function of the normalized time for different MO growth rate. T is the total loading time. (a) $W/h_{tc} = 4$, (b) $W/h_{tc} = 2$ and (c) $W/h_{tc} = 1$.

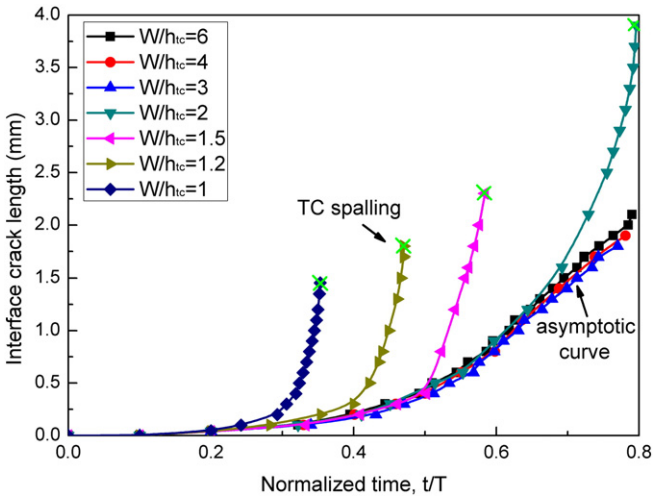

Fig. 8. The interface crack length as a function of the normalized time for different MO spaces. The green cross means the point at which TC spallation occurs. For relatively large MO space, there exists an asymptotic normalized loading time–crack length curve.

which means that the crack can easily propagate along the TGO/TC interface and then results in the premature spallation of coating.

It is worth noting in Fig. 9 that the critical MO space, also regarded as the breaking point of unsteady and steady state regions, is markedly affected by the current length of interface crack. In the case of the relatively short current length of the interface crack ($\bar{d} = 0.04$), the critical MO spaces approximately less than two times of the film thickness (e.g. $W/h_{TC} = 1.8$) and it rises to two times of the film thickness (e.g. $W/h_{TC} = 2$) as the crack length $\bar{d}$ increases to 0.2. The critical MO space is $W/h_{TC} = 3$ for a relatively long interface crack $\bar{d} = 0.5$. It can be concluded that the critical space of MO is significantly affected by the crack length and it appears to be enlarged as the interface crack extends. For a certain value of MO space (e.g. $W/h_{TC} = 2 \sim 3$), the interface delamination may not exhibit accelerative coalescence in the case of a small interface crack (e.g. $\bar{d} = 0.04$), but the coalescence may be possibly accelerated as the short crack propagates to a relatively long one (e.g. $\bar{d} = 0.5$). In the case of large MO space (i.e. $W/h_{TC} = 3$ to 6), the

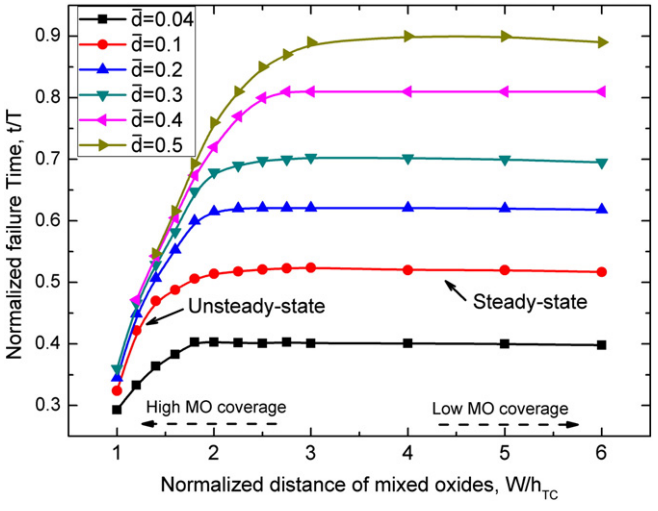

Fig. 9. The normalized failure time as a function of normalized MO space for different non-dimension crack lengths. For models of any given interface crack length with different MO spaces (also means different MO coverage at interface), there always exist two states: steady-state in which normalized failure time is independent on MO space, and unsteady-state in which the cracking behavior significantly depends on the MO space. The dependence in the unsteady-state indicates that the propagation of cracks in the model with relatively low MO space (also high MO coverage) will be dramatically promoted with the decrease of MO space (higher MO coverage).

studied herein, the spalling time of the coating becomes independent of MO space for a given crack length (see the steady state in Fig. 9). Over the critical value, the effect of MO space is not significant and can be neglected. Conversely, for a small MO space or in other words the high surface coverage ratio of MO, it has a notable effect on the spalling time for a given crack length. The normalized failure time drops dramatically with the decrease of MO space (see the unsteady state in Fig. 9),

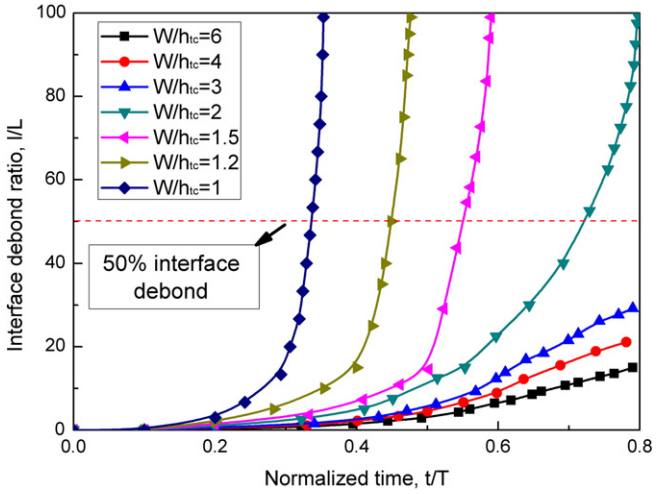

Fig. 10. The interfacial debonding ratio as a function of the normalized time for different MO spaces. The red dash line relates to 50% interfacial debonding, which is usually adopted to evaluate the failure of TBCs in thermal shock experiments.

crack gradually propagates to a sufficiently large size, which indicates that TBCs with large MO space (a low surface coverage ratio of MO) has good tolerance to interfacial delamination.

The interfacial debonding ratio η defined in Eq. (2) is an important parameter to characterize the interfacial failure behavior of TBCs. Fig. 10 shows the numerical results of η as a function of the normalized time for different MO space, which follows an intuitive expectation that TBCs with a small MO space at the interface have a higher interfacial debonding ratio than that with a large MO space at the surface. The reason has been discussed; see Figs. 8 and 9 for more details. In Fig. 10, we can also obtain the relationship between normalized loading time and interfacial debonding ratio. According to the previous experimental investigation [23], we use 50% interfacial debonding ratio as a critical value to define the TBCs failure, as the dash line in Fig. 10 shows. In this case, the normalized lifetime of TBCs equals to the normalized loading time when interfacial delamination reaches to 50%. So, we can plot the relationship between normalized lifetime and coverage ratio of MO, as shown in Fig. 11. Herein, the coverage ratio κ of MO at TGO/TC interface plays a key role in determining the normalized lifetime of TBCs. It is clear from Fig. 11 that the normalized lifetime of TBCs drops dramatically as the coverage ratio increases. That is why many

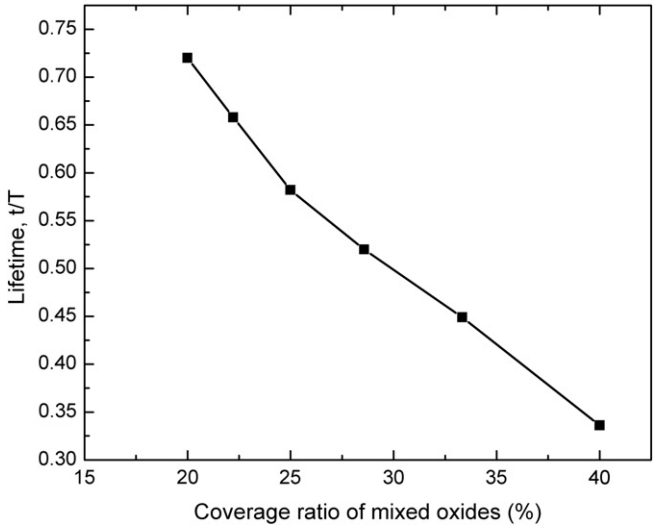

Fig. 11. The normalized lifetime versus the coverage ratio of MO.

experimental results show the normalized lifetime of TBCs is relatively low when there exist many MO at the interface [19,23,24,27]. Specifically, for TBCs with 40% coverage ratio of MO (calculated by Eq. (1) for the case of $W/h_{TC} = 1$), the normalized lifetime is about 0.33. However, for the TBCs with 20% coverage ratio of MO (for $W/h_{TC} = 2$), the normalized lifetime is 0.7 which is about twice the normalized lifetime of TBCs with 40% coverage ratio of MO. Therefore, it is concluded that the lifetime of TBCs can be improved effectively by reducing the coverage ratio of MO at interface. Li et al. [23] experimentally showed that the thermal cyclic lifetime of TBCs dramatically increases with the decrease of surface coverage of MO, which confirms the present numerical results. Moreover, Chen et al. [14,45] employed pre-oxidation treatments in low-pressure oxygen environments to suppress the formation of the detrimental MO. They found that the TBCs species with a low coverage rate of MO have better durability. The relation between lifetime and MO coverage rate shown in Fig. 11 can explain their experimental observation well.

One images from the above analysis that if we can control the oxygen environment during the depositing process of TBCs or choose a different thermal spray technique, then we can control the space of MO or in other words the surface coverage ratio of MO. And furthermore we can obtain long life TBCs. It is seen from Refs. [14,23,45] that this is possible but difficult.

5. Conclusion

The effect of mixed oxides (MO) growth on the interfacial fracture of the thermal barrier coating system (TBCs) is investigated in this work. A finite element model incorporating the "Debond" method and user subroutine *UEXPAN* in ABAUQS code is adopted to study the initiation and propagation of interfacial delamination.

It is concluded that MO has a deteriorative effect on the interface integrity of TBCs. The high growth rate of MO will induce a huge growth stress, subsequent interface crack propagation and eventual failure of TBCs. The high coverage ratio of MO will accelerate the propagation of the interface crack. Therefore, suppressing the formation of MO can effectively improve the durability and performance of TBCs.

The results obtained herein are in agreement with the previous experiments [23,27], can explain some failure phenomenon observed in experiments [14,18,21,23], and could offer the potential for improving the durability of TBCs.

Acknowledgments

This work is supported by the China 973 Program (2013CB035700) and NSFC (11321062, 11172227).

References

[1] R.A. Miller, Surf. Coat. Technol. 30 (1987) 1–11.
[2] N.P. Padture, M. Gell, E.H. Jordan, Science 296 (2002) 280–284.
[3] T.J. Wang, Z.W. Lou, Eng. Fract. Mech. 37 (1990) 825–829.
[4] T.J. Wang, Eng. Fract. Mech. 40 (1991) 1075–1082.
[5] T.J. Wang, Eng. Fract. Mech. 42 (1992) 177–183.
[6] T.J. Wang, Eng. Fract. Mech. 48 (1994) 217–230.
[7] E. Shillington, D. Clarke, Acta Mater. 47 (1999) 1297–1305.
[8] A.G. Evans, D. Mumm, J. Hutchinson, G. Meier, F. Pettit, Prog. Mater. Sci. 46 (2001) 505–553.
[9] X.L. Fan, W.X. Zhang, T.J. Wang, G. Liu, J. Zhang, Appl. Surf. Sci. 257 (2011) 6718–6724.
[10] X.L. Fan, R. Xu, W.X. Zhang, T.J. Wang, Appl. Surf. Sci. 258 (2012) 9816–9823.
[11] W.X. Zhang, X.L. Fan, T.J. Wang, Appl. Surf. Sci. 258 (2011) 811–817.
[12] A.M. Karlsson, A.G. Evans, Acta Mater. 49 (2001) 1793–1804.
[13] C.G. Levi, E. Sommer, S.G. Terry, A. Catanoiu, M. Rühle, J. Am. Ceram. Soc. 86 (2003) 676–685.
[14] W.R. Chen, X. Wu, B.R. Marple, D.R. Nagy, P.C. Patnaik, Surf. Coat. Technol. 202 (2008) 2677–2683.
[15] R. Xu, X.L. Fan, W.X. Zhang, Y. Song, T.J. Wang, Mater. Des. 47 (2013) 566–574.
[16] M. Martena, D. Botto, P. Fino, S. Sabbadini, M. Gola, C. Badini, Eng. Fail. Anal. 13 (2006) 409–426.
[17] M. Bialas, Surf. Coat. Technol. 202 (2008) 6002–6010.

[18] A. Rabiei, A.G. Evans, Acta Mater. 48 (2000) 3963–3976.
[19] K. Ogawa, K. Ito, T. Shoji, D. Seo, H. Tezuka, H. Kato, J. Therm. Spray Technol. 15 (2006) 640–651.
[20] M. Matsumoto, K. Hayakawa, S. Kitaoka, H. Matsubara, H. Takayama, Y. Kagiya, Y. Sugita, Mater. Sci. Eng. A 441 (2006) 119–125.
[21] M.S. Ali, S. Song, P. Xiao, J. Mater. Sci. 37 (2002) 2097–2102.
[22] O. Trunova, T. Beck, R. Herzog, R.W. Steinbrech, L. Singheiser, Surf. Coat. Technol. 202 (2008) 5027–5032.
[23] Y. Li, C.J. Li, Q. Zhang, G.J. Yang, C.X. Li, J. Therm. Spray Technol. 19 (2010) 168–177.
[24] A. Evans, D. Clarke, C. Levi, J. Eur. Ceram. Soc. 28 (2008) 1405–1419.
[25] S. Taniguchi, T. Shibata, A. Murakami, Oxid. Met. 41 (1994) 103–113.
[26] R.D. Maier, C.M. Scheuermann, C.W. Andrews, Am. Ceram. Soc. Bull. 60 (1981) 555–560.
[27] W. Chen, X. Wu, B.R. Marple, P.C. Patnaik, Surf. Coat. Technol. 197 (2005) 109–115.
[28] I. Zaplatynsky, National Aeronautics and Space Administration, 1971.
[29] Y. Ko, C. Chan, J. Eur. Ceram. Soc. 19 (1999) 2633–2639.
[30] J. Rösler, M. Bäker, K. Aufzug, Acta Mater. 52 (2004) 4809–4817.
[31] H. Zhu, N.A. Fleck, A.C.F. Cocks, A. Evans, Mater. Sci. Eng. A 404 (2005) 26–32.
[32] ABAQUS User's Manual, Dassault Systèmes Simulia Corporation, 2009.
[33] D. Mumm, A. Evans, I. Spitsberg, Acta Mater. 49 (2001) 2329–2340.
[34] W.X. Zhang, T.J. Wang, L.X. Li, Comput. Mater. Sci. 39 (2007) 684–696.
[35] J. Hutchinson, Z. Suo, Comput. Mater. Sci. 29 (1992) 191.
[36] F. McClintock, J. Appl. Mech. 25 (1958).
[37] J. Whitney, R. Nuismer, J. Compos. Mater. 8 (1974) 253–265.
[38] Y. Joliff, J. Absi, M. Huger, J. Glandus, Comput. Mater. Sci. 44 (2008) 826–831.
[39] M. Ranjbar-far, J. Absi, G. Mariaux, D.S. Smith, Mater. Des. 32 (2011) 4961–4969.
[40] V. Teixeira, M. Andritschky, W. Fischer, H.P. Buchkremer, D. Stöver, Surf. Coat. Technol. 120–121 (1999) 103–111.
[41] T.Q. Lu, W.X. Zhang, T.J. Wang, Int. J. Eng. Sci. 49 (2011) 967–975.
[42] M. He, A. Evans, J. Hutchinson, Mater. Sci. Eng. A 245 (1998) 168–181.
[43] H. Bhatnagar, S. Ghosh, M.E. Walter, Int. J. Solids Struct. 43 (2006) 4384–4406.
[44] M. S. Ali, S. Song, P. Xiao J. Eur. Ceram. Soc. 22(1) 101–107.
[45] W. Chen, R. Archer, X. Huang, BR. Marple. J. Thermal Spray Technol. 17(5) 858–864.